

# Loss Path Influence on the MRI Radio Frequency Pulse Sequence: A Theoretical Evidence

Moses Emeteré<sup>1,2\*</sup>, A Falade<sup>1</sup>

<sup>1</sup>*Covenant University, Ota, Nigeria;* <sup>2</sup>*Department of Mechanical Engineering Science, University of Johannesburg, Johannesburg, South Africa*

## Abstract

**Citation:** Emeteré N, Falade A. Loss Path Influence on the MRI Radio Frequency Pulse Sequence: A Theoretical Evidence. *Open Access Maced J Med Sci.* 2019 Sep 15; 7(17):2715-2722.  
<https://doi.org/10.3889/oamjms.2019.728>

**Keywords:** Loss Path Concept; Bloch NMR; Electromagnetic signatures; MRI; MRI antenna; Molecular interactions

**\*Correspondence:** Moses Emeteré, Covenant University, Ota, Nigeria. E-mail: [emeteré@yahoo.com](mailto:emeteré@yahoo.com)

**Received:** 29-May-2019; **Revised:** 23-Jul-2019; **Accepted:** 24-Jul-2019; **Online first:** 28-Aug-2019

**Copyright:** © 2019 Moses Emeteré, A Falade. This is an open-access article distributed under the terms of the Creative Commons Attribution-NonCommercial 4.0 International License (CC BY-NC 4.0)

**Funding:** This research did not receive any financial support

**Competing Interests:** The authors have declared that no competing interests exist

The RF pulse is initiated from either the loop or loopless MRI antenna. It has shown an increased advancement in recent times. Somehow, the concept has proven successful in the MR imaging procedure. Using the fundamental theories of the MRI concept, mathematical experimentation was carried out analytically to investigate the Loss Path Concept (LPC). The LPC was proposed to be one of the defects responsible for poor/blurred medical imaging of certain parts of the body. The LPC results obtain in this mathematical experimentation was found to be -56 dB and 6.7 dB. Theoretically, the LPC can be resolved mathematically by incorporating the molecular boundaries of the tissues. Practically, LPC can be resolved by introducing a detachable RF strip detector to synchronise-particles across different molecular boundaries and prevent patients from excess exposure to RF radiation.

## Introduction

Safe medical imaging is gradually advancing beyond mere visual interpretations of the interior parts of the human body into an improved technologically initiated process. This process includes improving the mathematical codes of the imaging device [1]. Mathematical codes are basic mathematical principles or algorithm used to initiate, construct or improve devices. These codes are rooted in sound physics principles to describe the functionality of devices. The operational techniques of the MRI machine are traceable to salient mathematical codes, e.g. the Bloch NMR. The mathematical codes of the MRI had been queried or faulted severally [2], [3]. Solutions had been inferred to the ab-initio mathematical codes of the MRI machines via recent inclusion of polynomial function [4], [5] to resolve imaging issues.

Therefore, mathematical codes can be used to probe into the complexity behind the functionality of the MRI machine. For example, aside from the known abnormalities in the MRI machine, i.e. signal-to-noise, excess heat on patients, increased radiation loss e.t.c., there are subtler issues about MRI that should be critically analysed. One of such salient challenge is the amount of signal attenuation recorded during radio propagation and reception. In this research, the signal attenuation anomaly is referred to as the loss path concept (LPC). LPC defines the performance (i.e. system frequency and link budget) of the radio propagation from the MRI antenna [6]. The MRI antenna transports energy into protons through resonance in the form of RF pulse. When the RF pulse is truncated, the excited protons return-back to its ab-initio state and emit RF signals. These signals are processed by the RF coil to generate tissue image on any output device, e.g. a computer. The image generation at the RF coil depends on the relaxation

time of hydrogen protons in different tissues (as shown in Figure 1).



Figure 1: MRI RF coils (adapted from [http://198.173.87.9/mri/mri\\_litzcagepg.htm](http://198.173.87.9/mri/mri_litzcagepg.htm))

Different medical resonance imaging processes [7], [8], [9] depend on the functionality of the MR antenna and the RF coils. These devices help to improve the acquisition and reconstruction of signal attenuation (as shown in Figure 2, A and B). Therefore, an antenna of large-quality factor and gain is required to provide a highly uniform electromagnetic field for high-resolution imaging.

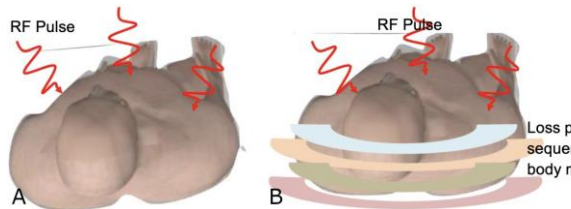


Figure 2: A) RF pulse from the MRI chamber; B) Loss Path in the RF Pulse Sequence

The constructive and destructive interference of electromagnetic fields generated by each part of the coil leads to low imaging [10]. This challenge has been reduced by introducing TEM resonators to control the distribution of the magnetic field [10]. It also assists meta/nano materials to focus on the RF magnetic field [11]. While solving the uniform distribution of the electromagnetic field, there exists the basic challenge of signal attenuation which leads to Loss Path Concept (LPC). LPC is as a result of continuous negligence of the Bio Savart law via the inadequate sustainability of the quality factor. Like 'shadow fading' in wireless capsule endoscopy [12], the Loss Path Concept (LPC) in the MRI is prominent when scanning deep tissues or cancerous growth of the human body. The RF attenuation when scanning deep tissues is a subtle concept. This concept was explained in subsequent sections of this paper. The relaxations of the excited protons of deep tissues are haphazardly different from general body imaging. This may be largely due to molecular interactions or boundaries of the deep tissues. Traditionally, the meta-material which act as the lens is used to focus on excess RF magnetic field to the patient to obtain

clearer imaging. Hence, the generalisation of the MRI procedure for body tissues should include the safety of the patient using the MRI machine.

The operational tendency for MRI technicians to subject patients to excessive RF radiation may be hazardous in the long-run [32]. This may lead to the weakening of body tissues and ultimately lead to organ malfunction e.t.c. Though none of these symptoms has been reported clinically, however, the essence of this research is to seek proactive measure – using a mathematical approach to probe the MRI technique. The LPC concept has been applied in some medical technologies, such as medical implant communication [19] and wireless capsule endoscopy [22]. In this paper, we developed a Hamiltonian to incorporate the shortcoming of the Bloch NMR model. The effects of electromagnetic signatures from the MRI antenna on the radio frequency (RF) are expected to excite both the selection technique and conservation of excess loss of energy during signalling. This concept was considered in the calculation. Also, the equations for the LPC were derived, and the simulated LPC effect during specific RF selection was reported.

## Material and Methods

The flow properties or fluid dynamics of the modified time-independent Bloch NMR flow equation under the influence of the RF magnetic field is given as [4], [5].

$$v^2 \frac{\partial^2 M_y}{\partial x^2} + v \left( \frac{1}{T_1} + \frac{1}{T_2} \right) \frac{\partial M_y}{\partial x} + \left( \frac{1}{T_1 T_2} + \gamma^2 B_1^2 \right) M_y - \frac{\gamma B_1 M_0}{T_1} = 0 \quad (1)$$

$v$  is the flow velocity.  $\gamma$  is the gyromagnetic ratio,  $M_y$  are the transverse magnetisation,  $M_z$  is the longitudinal magnetisation,  $M_0$  is the equilibrium magnetisation,  $x$  is the distance along the x-axis when time is not zero,  $B_1$  external magnetic field,  $T_1$  is the longitudinal and  $T_2$  transverse relaxation times.

The RF magnetic field is derived from antenna coils whose frequency is consistently higher than an amateur radio. The electromagnetic field from the antenna coils is governed by the Maxwell equations written below.

$$\nabla \cdot E = \frac{\rho}{\epsilon_0} \quad (2)$$

$$\nabla \times E = -\frac{\partial B}{\partial t} \quad (3)$$

$$\nabla \times B = \mu_0 J + \mu_0 \epsilon_0 \frac{\partial E}{\partial t} \quad (4)$$

$$\nabla \cdot \mathbf{B} = 0 \quad (5)$$

Equation (2) represents the Coulomb's law where  $\mathbf{E}$  is the electric field,  $\rho$  is the charge density,  $\epsilon_0$  is the permittivity of free space. Permittivity describes the ability of materials to transmit an electric field. Equation (3) represents the Faraday's law where  $\mathbf{B}$  is the magnetic induction. The negative sign can be justified using the Lenz law. Equation (4) is the Ampere's law where  $\mu_0$  is the permeability of free space. Permeability is the ability of a material to support the formation of a magnetic field within itself in response to an applied magnetic field.  $\mathbf{J}$  is the current density. Equation (5) represents the Gauss's law. The phenomena of both fields are the idea behind this paper.

**Enhanced Flow Parameters of the Bloch NMR Model**

We propose a generic Hamiltonian to incorporate the Bloch NMR and Molecular boundary dynamics as shown below

$$H_T = H_{Bloch} + H_{Molecular} \quad (6)$$

$H_{Bloch}$  is represented by the flow magnetisation equation derived by Awojogbe et al., [13]. The first step of this paper is to simplify the motion of the magnetisation vector in an externally polarised alternating magnetic field [26], [27], [28]. Secondly, the useful results are transferred to the rotating frame which mandates equation [1] not to be equal to zero. It is written as:

$$H_{Bloch} = v^2 \frac{\partial^2 M_y}{\partial x^2} + v \left( \frac{1}{T_1} + \frac{1}{T_2} \right) \frac{\partial M_y}{\partial x} + \left( \frac{1}{T_1 T_2} + \gamma^2 B_1^2 \right) M_y - \frac{\gamma B_1 M_0}{T_1} \quad (7)$$

The molecular boundary dynamics can also be expressed as:

$$H_{Molecular} = \frac{\partial E}{\partial x_i} \frac{\partial E}{\partial x_j} \quad (8)$$

All parameters maintain its original interpretations, i.e. E is the energy absorbed in the tissue. Along with the  $i^{th}$  site, the elastic model for macromolecular interactions is predominant because of body fluid, therefore,  $E = \sum_i^N V(x_i) + \sum_{i=2}^N \frac{1}{2} k(x_i - x_{i-1})^2$ , Along with  $j^{th}$  the site, the energy E coincide with the energy levels worked out by Emetere [14] for NMR studies.  $V(x_i)$  Is the potential across compartmental boundaries,  $x_i$  is the distance along in the  $i^{th}$  site in the x-axis,  $x_j$  is the distance along with the  $j^{th}$  site in the x-axis, N is the highest number of proton around

scanned body mass, k is the elasticity of the blood vessel. The elasticity of the arteries or blood vessel determines the blood flow rate in the body [15]. If the arteries are narrow, less blood can flow. In clinical practice, this feature is described by elasticity index.

Therefore the energy absorbed in the tissue is important for analysing both the microscopic and macroscopic imaging processes. Hence, the absorbed energy was represented by the ground energy level worked out by Emetere [14]  $E = 1 - m \cdot \omega_1 M_y T_1$  (9)

Here m is the magnetic moment. Assume  $m \cdot \omega_1 M_y T_1 \gg 1$ , i.e. when the external magnetic field is large; equation (8) can be further developed into equations (10 and 11).

$$\frac{\partial E}{\partial x_j} = \mu \cdot \omega_1 T_1 \frac{\partial M_y}{\partial x} \quad (10)$$

$$\frac{\partial E}{\partial x_i} = \sum_i^N \frac{\partial V(x_i)}{\partial x} + \sum_{i=2}^N \frac{1}{2} k(x_i - x_{i-1})^2 \quad (11)$$

This method is usually done in the matrix form, which is not the approach used in this section. The total Hamiltonian can be written as

$$H_T = v^2 \frac{\partial^2 M_y}{\partial x^2} + v \left( \frac{1}{T_1} + \frac{1}{T_2} + \mu \cdot \omega_1 T_1 \right) \frac{\partial M_y}{\partial x} + \sum_i^N \frac{\partial V(x_i)}{\partial x} + \left( \frac{1}{T_1 T_2} + \gamma^2 B_1^2 \right) M_y - \frac{\gamma B_1 M_0}{T_1} \quad (12)$$

We assume  $\sum_{i=2}^N \frac{1}{2} k(x_i - x_{i-1})^2 = 0$  for other tissues of the body, i.e. non- blood vessels because of its negligible elasticity. Applying the Schrödinger, i.e.  $H\psi = E\psi$ , equation [12] transforms into

$$v^2 M_y \frac{\partial^2 \psi}{\partial x^2} + \left[ v \left( \frac{1}{T_1} + \frac{1}{T_2} + \mu \cdot \omega_1 T_1 \right) M_y + \sum_i^N V(x_i) \right] \frac{\partial \psi}{\partial x} + \left[ \left( \frac{1}{T_1 T_2} + \gamma^2 B_1^2 \right) M_y - E - \frac{\gamma B_1 M_0}{T_1} \right] \psi = 0 \quad (13)$$

$\psi$  Have been calculated by Emetere [14], [25] in a generalised form as  $\psi = A \exp(i\omega t)$ . To analyse the time-independent domain,  $t = \frac{xr}{\omega}$ , where  $x$  is the circumference of the base sector of the coil,  $r$  is the radial component. Therefore,

$$\psi = A \exp(ixr) \quad (14)$$

Substituting equation (14) into equation (13) yields two sets of governing equations

$$v^2 r^2 M_y + \left( \frac{1}{T_1 T_2} + \gamma^2 B_1^2 \right) M_y - E - \frac{\gamma B_1 M_0}{T_1} = 0 \quad (15a)$$

$$v \left( \frac{1}{T_1} + \frac{1}{T_2} + \mu \cdot \omega_1 T_1 \right) M_y + \sum_i^N V(x_i) = 0$$

(15b)

The governing equations yield the following solutions

$$M_y = \frac{ET_1T_2 + \gamma B_1 M_0 T_2}{v^2 r^2 T_1 T_2 + 1 + \gamma^2 B_1^2 T_1 T_2} \quad (15c)$$

$$M_y = \frac{T_1 T_2 \sum_i^N V(x_i)}{(\tau + \mu \omega_1 T_1^2 T_2) v} \quad (15d)$$

Where  $\tau = T_1 + T_2$ . If a low relaxation of the excited proton is considered, then  $v^2 r^2 T_1 T_2 \ll 1$  and  $ET_1 T_2 \ll 1$ . Equation (15c) becomes,

$$M_y = \frac{\gamma B_1 T_2 M_0}{1 + \gamma^2 B_1^2 T_1 T_2} \quad (15e)$$

Equation (15e) is the exact solution of the continuous wave nuclear magnetic resonance (CW NMR) and is expressed in the laboratory frame as

$$M_{x0} = \frac{-\sin(\omega t) \gamma B_1 T_2 M_0}{1 + \gamma^2 B_1^2 T_1 T_2} \quad (16a)$$

$$M_{y0} = \frac{\cos(\omega t) \gamma B_1 T_2 M_0}{1 + \gamma^2 B_1^2 T_1 T_2} \quad (16b)$$

This result had been reported by numerous researchers (16, 17), i.e. showing the validity of our approach. Also, if we consider a high relaxation of the excited proton, then  $\mu \omega_1 T_1^2 T_2 \gg \tau$ , equation (15d) yields a new exact solution of the CW NMR i.e.

$$M_y = \frac{\sum_i^N V(x_i)}{\mu \omega_1 T_1 v} \quad (17)$$

The exact solution of CW NMR in a laboratory frame can also be written as

$$M_{x0} = \frac{-\sin(\omega t) \sum_i^N V(x_i)}{\mu \omega_1 T_1 v} \quad (18)$$

$$M_{y0} = \frac{\cos(\omega t) \sum_i^N V(x_i)}{\mu \omega_1 T_1 v} \quad (19)$$

The processes highlighted in equations (16a and 16b) and equations (18 and 19) are driven by the concept discussed in the succeeding section.

## Results

The time-independent Schrödinger equation was modelled to open up the proton's dynamics initiated by the MRI antenna. The time-independent Schrödinger equation is given as

$$i\hbar \frac{\partial}{\partial t} \psi - \frac{\hbar^2}{2m} \nabla^2 \psi + V\psi = 0 \quad (20)$$

The Lagrangian density which shows the functionality between the transmitting and receiving

antenna coil (equation [24]) is given as

$$\mathcal{L}_1 = \frac{1}{2} \left[ \left| \frac{\partial \psi}{\partial t} \right|^2 - \frac{\hbar^2}{2m} |\nabla \psi|^2 - V|\psi|^2 \right] \quad (21)$$

The minimum coupling rule to describe the interaction of  $\psi$  with the electromagnetic field was applied to get

$$\frac{\partial}{\partial t} \mapsto \frac{\partial}{\partial t} + ieV, \quad \nabla \mapsto \nabla - ieA \quad \text{where} \\ V = V(r, \theta) = V_0 + E_0 \left( \frac{a^2}{r} - r \right)$$

Where  $V_0$  is a constant on the surface of the faraday loop of the MRI antenna,  $E_0$  is the field,  $r$  is the radius of the antenna, 'a' is the radius of the RF circular loop. Here, it is assumed that the shape of the antenna is loop-like.

Equation [25] transforms into

$$\mathcal{L}_1 = \frac{1}{2} \left[ \left| \frac{\partial \psi}{\partial t} + ie\psi\phi \right|^2 - \frac{\hbar^2}{2m} |\nabla \psi - ieA\psi|^2 - V|\psi|^2 \right] \quad (22)$$

The circular conductor is accounted for where  $r = x$

$$\mathcal{L}_1 = \frac{1}{2} \left[ \left| \frac{\partial \psi}{\partial t} + ie\psi V_0 + iE_0 e\psi \left( \frac{a^2}{x} - x \right) \cos \omega t \right|^2 - \frac{\hbar^2}{2m} |\nabla \psi - ieA\psi|^2 - V|\psi|^2 \right] \quad (23)$$

Applying the solution of the standing wave  $\psi(x, t) = e^{iS(x,t)} T(x, t)$  in equation [4]

Where  $E, B: \mathbb{R}^3 \times \mathbb{R} \rightarrow \mathbb{R}$ , the lagrangian density takes the form

$$\mathcal{L}_1 = \frac{1}{2} \left[ E_t^2 - |E_z|^2 - \left[ \frac{\hbar^2}{2m} |B_r - eA|^2 + |B_z + V_0 e|^2 - \left( |B_z - E_0 e \left( \frac{a^2}{x} - x \right) \right)^2 - |B_z|^2 \right] + 2E_0 V_0 e^2 \right] E_r^2 \quad (24)$$

Considering the Lagrangian density of the particle electromagnetic field E-H field of the circular MRI antenna-coil,

$$\mathcal{L}_0 = \frac{1}{8\pi} (|E_1|^2 - |E_2|^2 - |H_1|^2 - |H_2|^2) \quad (25)$$

Where the values of electric and magnetic were adapted from Glenn (18) and restructured into the circular MRI loop antenna

$$E_1(a, z) = (\beta E_r(a, z) e_r + E_z(a, z) e_z) e^{-j\beta r \sin \theta} \quad (26)$$

$$E_2(a, z) = (\beta E_r(a, z) e_{r1} + E_z(a, z) e_{z1}) e^{-j\beta r \cos \theta} \quad (27)$$

$$H_1(a, z) = (\beta B_r(a, z) f_r + B_z(a, z) f_z) e^{-j\beta r \sin \theta} \quad (28)$$

$$H_2(a, z) = (\beta B_r(a, z) f_{r1} + B_z(a, z) f_{z1}) e^{-j\beta r \cos \theta} \quad (29)$$

Where  $e_r = e_{r1} = \frac{\xi m}{4\pi r}$  and  $e_z = e_{z1} = \frac{\xi m j}{4\pi z^2}$  ;  $f_r = f_{r1} = \frac{\mu_0 m j}{4\pi r^2}$  and  $f_z = f_{z1} = \frac{\mu_0 m}{4\pi z^3}$

Beyond the mere introduction of boundary conditions to expatiate on the dynamics of equations [26-29], its 'real-time' applications include reducing computational challenges (when writing the mathematical codes (1)) and micro-analysis of the selection technique.

The boundary conditions for equation [26] are

$$\begin{cases} E_1(a, 0) = E_\alpha(z) \\ E_1(\infty, z) = 0 \\ E_1(a, x) = E_\alpha(z) \cdot \alpha \\ E_1(a, \infty) = 0 \end{cases} \quad (30)$$

The boundary conditions for equation [27] are

$$\begin{cases} E_2(a, 0) = E_\gamma(z) \\ E_2(\infty, z) = 0 \\ E_2(a, x) = E_\gamma(z) \cdot \gamma \\ E_2(a, \infty) = 0 \end{cases} \quad (31)$$

The boundary conditions for equation [28] are

$$\begin{cases} B_1(a, 0) = B_\vartheta(z) \\ B_1(\infty, z) = 0 \\ B_1(a, x) = B_\vartheta(z) \cdot \vartheta \\ B_1(a, \infty) = 0 \end{cases} \quad (32)$$

The boundary conditions for equation [29] are

$$\begin{cases} B_2(a, 0) = B_\sigma(z) \\ B_2(\infty, z) = 0 \\ B_2(a, x) = B_\sigma(z) \cdot \sigma \\ B_2(a, \infty) = 0 \end{cases} \quad (33)$$

where  $\alpha$  and  $\gamma$  are the attenuation factors of the electrical fields;  $\sigma$  and  $\vartheta$  are the attenuation factors of the magnetic fields;  $B_\vartheta(z)$  and  $B_\sigma(z)$  are the magnetic fields at the boundary of the MRI antenna;  $E_\gamma(z)$  and  $E_\alpha(z)$  are the electric fields at the boundary of the MRI antenna;  $x$  is the length of MRI antenna;  $\beta$  is the frequency of excited power;  $j$  is the radio frequency current;  $r$  represents the radius or horizontal component of the antenna;  $z$  represents the vertical component of the antenna;  $m$  represents the number of the protons;  $\xi$  represents the electrical permeability;  $\mu_0$  represents the magnetic permeability;  $e_r$  is the spin factor which determines the protons spin along the horizontal component of the MRI;  $e_z$  is the spin factor which determines the protons spin along the vertical component of the MRI transmitting antenna;  $e_{r1}$  is the spin factor which

determines the protons spin along the horizontal component within the electric field of the MRI receiving antenna;  $e_{z1}$  is the spin factor which determines the protons spin along the vertical component within the electric field of the MRI transmitting antenna;  $f_r$  is the spin factor which determines the protons spin along the horizontal component within the magnetic field of the MRI receiving antenna;  $f_{r1}$  is the spin factor which determines the protons spin along the horizontal component within the magnetic field of the MRI transmitting antenna;  $f_z$  is the spin factor which determines the protons spin along the vertical component within the magnetic field of the MRI receiving antenna;  $f_{z1}$  is the spin factor which determines the protons spin along the vertical component within the magnetic field of the MRI transmitting antenna.

Therefore, the total action of lagrangian density is given by

$$D = \iint \mathcal{L}_1 + \mathcal{L}_0 \quad (34)$$

Then the Euler-Lagrange equation associated to the function  $S = S(E_r, E_z, B_r, B_z, r, \theta, z)$  gives rise to the following systems of equation

$$E_r + \left[ \frac{\hbar^2}{2m} |B_r - eA|^2 + |B_z + V_0 e|^2 - (|B_z - E_0 e \left( \frac{a^2}{r^2} - r \right)|^2 - |B_z|^2) + 2E_0 V_0 e^2 + \beta e_r \right] E_r = \beta E_r e_r e^{-j\beta r} (\sin\theta + \cos\theta) \quad (35)$$

$$\frac{\partial}{\partial t} [(B_z + V_0 e) E_r^2] - \frac{\partial}{\partial t} \left[ \left( B_z + E_0 e \left( \frac{a^2}{x} - x \right) \right) E_r^2 \right] - \frac{1}{2} \frac{\partial B_z}{\partial t} = 0 \quad (36)$$

$$\frac{\hbar^2}{2m} E_r^2 \frac{\partial}{\partial t} (B_r - eA) = \beta B_r f_r e^{-j\beta r} (\sin\theta + \cos\theta) \quad (37)$$

$$\frac{\partial}{\partial t} E_z = \frac{\partial}{\partial t} E_z e_z e^{-j\beta r} (\sin\theta + \cos\theta) \quad (38)$$

$$2 |B_z - E_0 e \left( \frac{a^2}{r} - r \right)| E_r E_0 e \left( \frac{a^2}{r^2} - 1 \right) = \frac{j\beta}{8\pi} \left[ \frac{E_r E_r}{r} (\sin\theta + \cos\theta) + \frac{2B_r f_r}{r} (\sin\theta + \cos\theta) \right] \beta e^{-j\beta r} \quad (39)$$

$$\frac{1}{8\pi} [\beta E_r(a, z) e_r + \beta B_r(a, z) f_r + E_z(a, z) e_z + B_z(a, z) f_z] [\cos\theta - \sin\theta] = 0 \quad (40)$$

$$\frac{1}{8\pi} [-\frac{2}{z} e^{-j\beta r} \sin\theta (B_z(a, z) f_z + E_z(a, z) e_z) - \frac{2}{z} e^{-j\beta r} \cos\theta (B_z(a, z) f_z + E_z(a, z) e_z)] = 0 \quad (41)$$

## Discussion

RF pulses are required to attain transverse magnetisation (equation 16b & 19). This can be initiated via the electromagnetic signatures expressed in equation [37]. We can easily obtain any solution of

the transverse magnetisation (when  $\theta = \omega t; B_r = M_{y0}$ ) via this method

$$\omega \left( -\frac{\hbar^2}{2m\beta f_r} E_r^2 \right) e^{j\beta r} = \cos\omega t + \cos^2\omega t \tag{42}$$

Equation [42] is related to the loss path equation stated by Basar et al., (19) where  $j\beta r$  is the loss path,  $\cos\theta + \cos^2\theta$  is the cumulative spin precession angle,  $\frac{\hbar^2}{2m\beta f_r} E_r^2 = K$  is the RF pulse sequence,  $\omega$  is the frequency. Taking the assumption that LPC was stated in equation (42)  $\frac{j\beta r}{20}$ , then the distance between the transmitting and receiving points are determined, as shown in Figure 7. Hence, the transformed equation (42) can be written as

$$LPC = 20 \log_K \left( -\frac{\cos\omega t + \cos^2\omega t}{\omega} \right) \tag{43}$$

The cumulative spin precession angle can be determined from the combination of deviated spins along with the same phase (as shown in Figure 3 below). A typical effect of the cumulative spin precession angle of individual protons in the human body Figure 3.

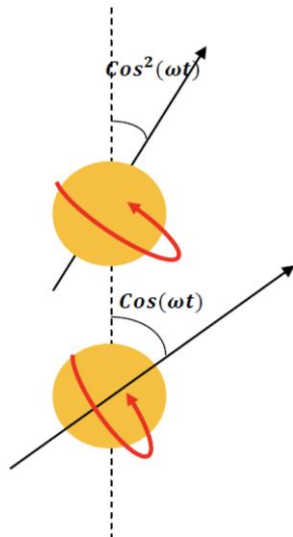


Figure 3: Physical model of cumulative spin precession angle

The MRI machine transmits a different pulse sequence (Figure 2B) when scanning a specific body mass. The pulse sequence through the free space and its losses are dependent on the frequency that was derived in equation [42]. The loss path has the same properties as the RF pulse sequence (i.e. frequency of exciting power) and differs from the usual loss path property that describes the transmitted power [19]. The linear dependence of the RF pulse, loss path and cumulative spin precession was investigated (Figure 4).

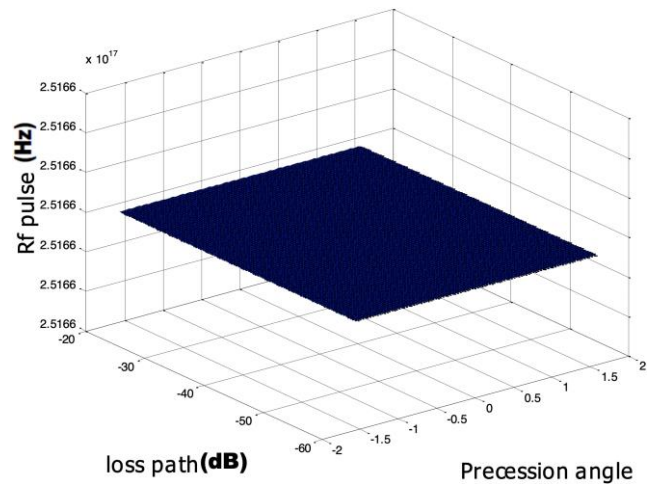


Figure 4: linearly dependence of the RF pulse, loss path and cumulative spin precession. A decrease in frequency translates in an increase in the RF pulse

The basis of linearity was initiated by the sudden decrease in the frequency of protons. These protons in the tissues increase the tendency of RF pulse to create imaging impact and vice-versa. The normal distribution of the RF pulse over tissues is represented in Figure 5.

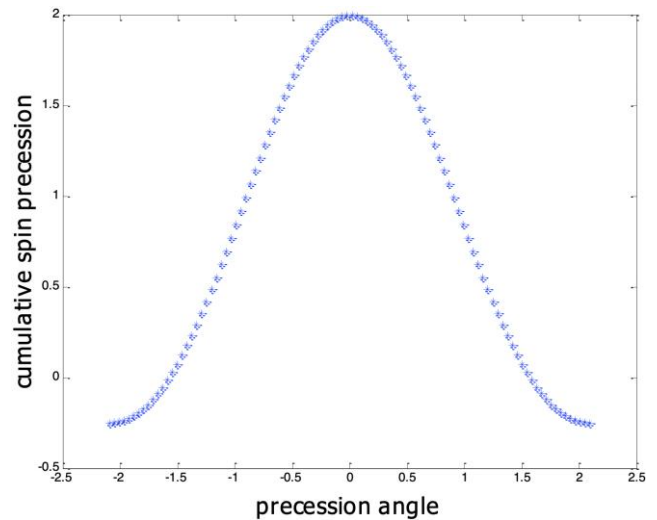


Figure 5: Distribution of RF for deep tissue analysis

Experimentally, the distribution of the RF pulse is not a smooth curve [20], [21]. One of the reasons attributed to this occurrence is the electromagnetic signatures of the MRI antenna. Recall the importance of the electromagnetic signatures had been mathematically illustrated in section three. The electromagnetic signatures are the specific combination of emitted, reflected or absorbed electromagnetic radiation (EM) at varying wavelengths and directions. This concept defines a unique set of combined frequencies, as seen in the loss path. Equation [42] is a typical electromagnetic signature of the MRI antenna. In a narrow view, i.e. at the low quantity of electromagnetic radiation, the system is

excited by differential amount of electrical energy. In a practical sense, the electromagnetic radiation in the MRI is moderate. The description of moderate electromagnetic radiation may be relative, i.e. depending on the operational specifics of the MRI machine. Practically, the energy in MRI operations is controlled by the integration of the function of equation [42] to account for the many-body effects shown in Figure 4 and 6 below. Since a safe MRI operation was assumed, the extremes of the equation [42] were not explained in this paper.

Practically, the determination of the RF value for deep tissue analysis is equal to the shadow fading for deep tissue implant [22] as shown in Figure (5). The effects of the RF pulse attenuation at varying frequencies were investigated (Figure 6A, B, C, and D). The RF pulse attenuation decreases at higher frequencies. At higher loss path, the RF pulse decreases drastically. The LPC for this mathematical experimentation of the MR process was found to be -56 dB and -20 dB. Further calculation of the LPC value using equation (43) could be extended to 6.7 dB.

It is easy to infer from Figure (6 A, B, C, and D), that the electromagnetic signature creates a non-uniform impact on the protons of the body. This phenomenon results in a process called quasi-resonance. In the quasi resonance state, all the protons do not come under the same influence of the radio frequency. This is partly because of the LPC. For easy identification, such protons are referred to as 'vagabond' protons. They reside mainly at the molecular boundaries and partially absorb the radio frequencies that in turn obstruct the transverse magnetisation signals. Hence, it was proposed that LPC could be initiated by the potential between molecular boundaries.

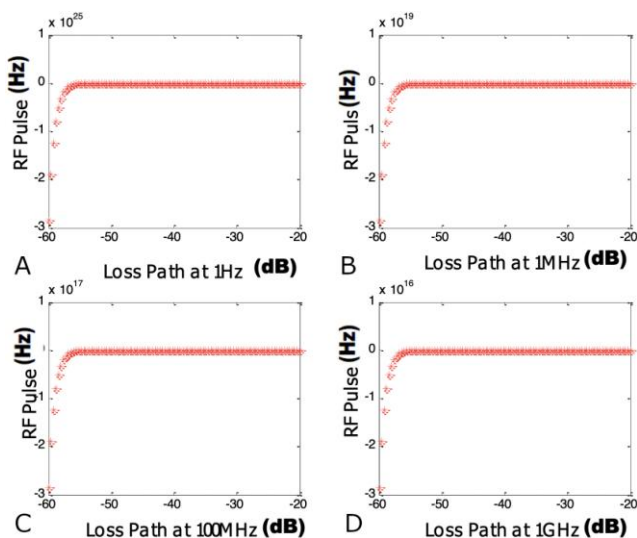


Figure 6: RF pulse attenuation at varying frequencies

The non-inclusion of the potential across molecular boundaries in the ab-initio Bloch NMR

equations (23-29) conceals the error due to the existence of the 'vagabond' proton that resides in some tissues or tumours (Figure 7). The excess ejection of heat (due to the 'vagabond' protons at the molecular boundaries) is one of the challenges in MRI.

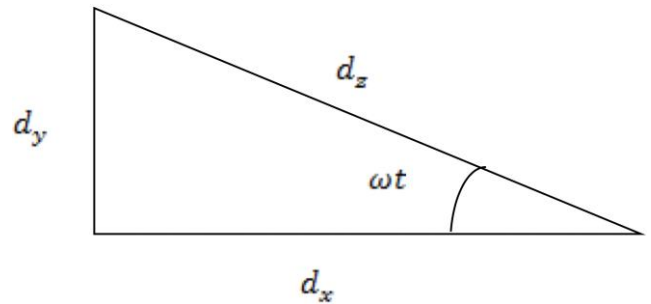


Figure 7: Angular resolution of the distance between the transmitting and receiving points

The 'vagabond' protons trap excesses energy as shown in equation [42]. Since the principle of conservation of energy must be obeyed, the 'vagabond' proton ejects the trapped energy in the form of heat. Some scientists and engineers had suggested that the challenges of MRI signal attenuation could be remedied by introducing the loopless MRI antenna [30] and MRI strip detectors [31], [32]. This idea is very effective to improve the signal-to-noise ratio (SNR) and field-of-view (FOV).

The LPC exists in the MR process. This can be seen in the reduction in RF pulse at higher frequencies. The LPC for MR processes was found to be -56 dB and 6.7 dB. The existence of the LPC led to another concept like the existence of the 'vagabond' proton. It was reported that the 'vagabond' proton supports poor imaging from the MR process. The LPC exposes the danger of improper design of the RF sequence. This fundamental error exposes the patient to a higher frequency that may be abnormal for certain regions of the body. Theoretically, incorporating the molecular boundaries potentials in the ab-initio MRI source code can solve the LPC. Practically, LPC can be resolved by introducing a detachable device like RF strip detector that would synchronise particles across different molecular boundaries and prevent patients from excessive exposure to high RF frequencies.

## Acknowledgement

The author appreciates the supports of J. Emetere. The author appreciates the initial discussion with Prof. O. B. Awojoyogbe. The author acknowledges Covenant University.

## References

1. Siegmund, J, et al. Understanding Understanding Source Code with Functional Magnetic Resonance Imaging. Proceedings of the 36th ACM/IEEE International Conference on Software Engineering. 2014; 378-389. <https://doi.org/10.1145/2568225.2568252>
2. Schmithorst VJ, Brown RD. Empirical validation of the triple-code model of numerical processing for complex math operations using functional MRI and group Independent Component Analysis of the mental addition and subtraction of fractions. *Neuroimage*. 2004; 22(3):1414-20. <https://doi.org/10.1016/j.neuroimage.2004.03.021> PMID:15219612
3. Mitsouras D, Hoge WS, Rybicki FJ, Kyriakos WE, Edelman A, Zientara GP. Non-Fourier-encoded parallel MRI using multiple receiver coils. *Magnetic Resonance in Medicine: An Official Journal of the International Society for Magnetic Resonance in Medicine*. 2004; 52(2):321-8. <https://doi.org/10.1002/mrm.20172> PMID:15282814
4. Awojoyogbe OB, et al. Mathematical Models of real Geometrical Factors in Restricted Blood vessels for the Analysis of CAD (Coronary Artery Diseases) Using Legendre, Boubaker and Bessel polynomials *J Med Syst*. 2010; 9:9428. <https://doi.org/10.1007/s10916-009-9428-9> PMID:20703766
5. Emeteri ME, Akinyemi ML. A Model for Resolving Flow Parameters for MRI- Neuroimaging Application, *American Journal of Applied Sciences*. 2015; 12(9):627-635. <https://doi.org/10.3844/ajassp.2015.627.635>
6. Phaebua K, et al. Path-loss prediction of radio wave propagation in an orchard by using modified UTD method, *Progress In Electromagnetics Research*. 2012; 128:347-363. <https://doi.org/10.2528/PIER12040106>
7. Özarslan E, Mareci TH. Generalized diffusion tensor imaging and analytical relationships between diffusion tensor imaging and high angular resolution diffusion imaging. *Magnetic Resonance in Medicine: An Official Journal of the International Society for Magnetic Resonance in Medicine*. 2003; 50(5):955-65. <https://doi.org/10.1002/mrm.10596> PMID:14587006
8. Wedeen VJ, Hagmann P, Tseng WY, Reese TG, Weisskoff RM. Mapping complex tissue architecture with diffusion spectrum magnetic resonance imaging. *Magnetic resonance in medicine*. 2005; 54(6):1377-86. <https://doi.org/10.1002/mrm.20642> PMID:16247738
9. Descoteaux M, et al. Regularized, fast, and robust analytical q-ball imaging. *Magnetic Resonance in Medicine*. 2007; 58:497-510. <https://doi.org/10.1002/mrm.21277> PMID:17763358
10. Pang Y, Xie Z, Xu D, Kelley DA, Nelson SJ, Vigneron DB, Zhang X. A dual-tuned quadrature volume coil with mixed  $\lambda/2$  and  $\lambda/4$  microstrip resonators for multinuclear MRSI at 7 T. *Magnetic resonance imaging*. 2012; 30(2):290-8. <https://doi.org/10.1016/j.mri.2011.09.022> PMID:22055851 PMID:PMC3254778
11. Pang Y, Xie Z, Li Y, Xu D, Vigneron D, Zhang X. Resonant mode reduction in radiofrequency volume coils for ultrahigh field magnetic resonance imaging. *Materials*. 2011; 4(8):1333-44. <https://doi.org/10.3390/ma4081333> PMID:22081791 PMID:PMC3212035
12. Iddan G, Meron G, Glukhovskiy A, Swain P. Wireless capsule endoscopy. *Nature*. 2000; 405(6785):417. <https://doi.org/10.1038/35013140> PMID:10839527
13. Awojoyogbe OB. Analytical solution of the time-dependent Bloch NMR flow equations: a translational mechanical analysis. *Physica A: Statistical Mechanics and Its Applications*. 2004; 339(3-4):437-60. <https://doi.org/10.1016/j.physa.2004.03.061>
14. Emeteri M. Mathematical Modelling of Bloch NMR to Solve the Schrödinger Time Dependent Equation. *The African Review of Physics*. 2013; 8:65-8. <https://doi.org/10.12988/ams.2014.4012>
15. Qi H, Bai X, Zhou H, Wu B. Elasticity of blood vessel decreased induced by aging is the main factor of vascular senescence. *Heart*. 2012; 98(Suppl 2):E146. <https://doi.org/10.1136/heartjnl-2012-302920d.32>
16. Odoh EO, De DK. Application of Nuclear Magnetic Resonance Imaging in Blood Flow Estimation. *The African Physical Review*. 2009; 3:65-74.
17. De DK. NMR/MRI Blood Flow Magnetization Equation in the Rotating Frame of Reference: Part I. *The African Physical Review*. 2013; 8:201.
18. Glenn SS. Radiation Efficiency of Electrically Small Multiturn Loop Antennas *IEEE Trans Antennas Propagat*. 1972; 20(5) 656-657(1972). <https://doi.org/10.1109/TAP.1972.1140293>
19. Basar MR, Malek MF, Juni KM, Saleh MI, Idris MS, Mohamed L, Saudin N, Mohd Affendi NA, Ali A. The use of a human body model to determine the variation of path losses in the human body channel in wireless capsule endoscopy. *Progress In Electromagnetics Research*. 2013; 133:495-513. <https://doi.org/10.2528/PIER12091203>
20. Scheffler K. A pictorial description of steady-states in rapid magnetic resonance imaging. *Concepts in Magnetic Resonance: An Educational Journal*. 1999; 11(5):291-304. [https://doi.org/10.1002/\(SICI\)1099-0534\(1999\)11:5<291::AID-CMR2>3.0.CO;2-J](https://doi.org/10.1002/(SICI)1099-0534(1999)11:5<291::AID-CMR2>3.0.CO;2-J)
21. Tannús A, Garwood M. Adiabatic pulses. *NMR in Biomedicine: An International Journal Devoted to the Development and Application of Magnetic Resonance In Vivo*. 1997; 10(8):423-34. [https://doi.org/10.1002/\(SICI\)1099-1492\(199712\)10:8<423::AID-NBM488>3.0.CO;2-X](https://doi.org/10.1002/(SICI)1099-1492(199712)10:8<423::AID-NBM488>3.0.CO;2-X)
22. Kamran S-P, et al. A Statistical LPC Model for Medical Implant Communication Channels. *Personal, Indoor and Mobile Radio Communications, IEEE 20th International Symposium, 2009:2995 - 2999*
23. Uno UE, Emeteri M. Analysis of the high temperature superconducting magnetic penetration depth using the Bloch NMR equations. *Global engineers & technologists review*. 2012; 2(1):14-21.
24. Emeteri M. Mathematical modelling of Bloch NMR to explain the Rashba Energy Features. *World Journal of Condensed Matter Physics*. 2013; 3:87-94. <https://doi.org/10.4236/wjcmp.2013.31015>
25. Emeteri, Moses E., 2014. Mathematical Modeling of Bloch NMR to Solve a Three Dimensional- Schrodinger Time Dependent Equation. *Applied Mathematical Sciences* 8, 2753 – 2762. <https://doi.org/10.12988/ams.2014.4012>
26. Emeteri M. Quantum information technology based on magnetic excitation of single spin dynamics. *Industrial Engineering Letters*. 2013; 3(5):33-36
27. Emeteri ME, Uno UE, Isah K. A remodeled stretched exponential-decay formula for complex systems. *Research & reviews: journal of engineering and technology*. 2014; 3(2):4-12.
28. Emeteri ME. Characteristic significance of magnetic relaxations on copper oxide thin film using the Bloch NMR. *Surface Review and Letters*. 2014; 21(05):1450075. <https://doi.org/10.1142/S0218625X14500759>
29. Emeteri M, Bakeko M. Determination of Characteristic Relaxation Times and Their Significance in A Copper Oxide Thin Film. *Journal of Theoretical Physics and Cryptography*. 2013;4:1-4.
30. Attig N, et al. John von Neumann Institute for Computing, Jülich, NIC Series. 2004; 23:1-28.
31. Kumar A, Bottomley PA. Optimizing the intrinsic signal-to-noise ratio of MRI strip detectors. *Magnetic Resonance in Medicine: An Official Journal of the International Society for Magnetic Resonance in Medicine*. 2006; 56(1):157-66. <https://doi.org/10.1002/mrm.20915> PMID:16724302 PMID:PMC2094217
32. Schilling CJ. Effects of exposure to very high frequency radiofrequency radiation on six antenna engineers in two separate incidents. *Occupational medicine*. 2000; 50(1):49-56. <https://doi.org/10.1093/occmed/50.1.49> PMID:10795393